THE JOURNAL OF BIOLOGICAL CHEMISTRY VOL. 281, NO. 35, pp. 25612–25621, September 1, 2006

Solution Structure and Antiestrogenic Activity of the Unique C-terminal, NR-box Motif-containing Region of MTA1s*

Received for publication, May 10, 2006, and in revised form, June 26, 2006 Published, JBC Papers in Press, June 27, 2006, DOI 10.1074/jbc.M604444200

Rajesh R. Singh[‡1], Kumaralal Kaluarachchi[§1], Mingzhi Chen[¶2], Suresh K. Rayala[‡], Seetharaman Balasenthil[‡], Jianpeng Ma[¶‖3], and Rakesh Kumar[‡ ‡‡4]**

*From the [‡]Department of Molecular and Cellular Oncology and [§]Experimental Therapeutics, University of Texas M.D. Anderson Cancer Center, Houston, Texas 77030, the [¶]Graduate Program of Structural and Computational Biology and Molecular Biophysics, Baylor College of Medicine, Houston, Texas 77030, the **Department of Bioengineering, Rice University, Houston, Texas 77251, the [‖]Verna and Marrs McLean Department of Biochemistry and Molecular Biology, Baylor College of Medicine, Houston, Texas 77030, and the [‡‡]Department of Molecular and Cellular Biology, Baylor College of Medicine, Houston, Texas 77030*

Metastasis tumor-associated 1 short form (MTA1s) is a naturally occurring, alternatively spliced variant of MTA1 that functions as a repressor of estrogen receptor (ER) α transcriptional functions, at least in part by binding and sequestering ERα in the cytoplasm. A unique C-terminal 33-amino acid region containing a nuclear receptor (NR)-box motif (-LRILL-) mediates binding of MTA1s with ERα and is indispensable in this interaction. Here, we elucidated the solution structure of this 33-amino acid region by NMR spectroscopy. We found a predominance of the α-helical region toward the N-terminal region, which includes the NR-box motif. *In silico* docking and comparison studies showed similarities between the NR-box motif of MTA1s and a similar motif of coregulators, both in structure and mode of ERα binding. In MCF-7 breast cancer cells, the MTA1s peptide effectively repressed ERα transactivation function, as evidenced by the estrogen response element-luc assay and down-regulation of estrogen-induced genes. In mechanistic studies, we found that the antiestrogenic effects of the MTA1s peptide were due to its ability to compete with the coactivator recruitment to ERα. Furthermore, the peptide efficiently repressed estrogen-induced proliferation and anchorage-independent growth of MCF-7 cells. In addition, the MTA1s peptide blocked the progression of tumors formed by MCF-7 cells overexpressing an ERα coactivator in a xenograft-based assay. In brief, the characterization of structure and antiestrogenic activity of MTA1s peptide highlight its therapeutic potential.

Protein-protein interactions play an important role in communicating signals in the cell, which involves the conductance and amplification of the message from a master hormonal signal. In this context, the proteins involved in the downstream convergence of the signals are equipped with specialized domains that help establish specific inter-protein interactions to achieve high signal transduction efficiency. In recent years, extensive research on proteins such as the nuclear receptor (NR)[5] family of hormone-induced transcription factors has identified their mode of action and their binding partners, providing novel insights into the significance of specialized protein-protein interactions in hormone action.

The NR family is composed of ~48 structurally related transcription factors, which require their cognate ligand for activity. Upon ligand binding, the NR homodimers or heterodimers selectively bind to the specific short stretches of DNA, referred to as hormone response elements, and stimulate transcription of the target genes responsible for vital biological processes such as cell survival, proliferation, differentiation, and apoptosis (1).

NRs are composed of structurally and functionally similar molecular domains, which reflect their common mode of action. The N-terminal domain is referred to as "activation function 1" (AF1), which shows a higher degree of sequence variation. NRs also have a highly conserved central DNA-binding domain composed of two zinc finger motifs. The ligand-binding domain to which the hormones bind is localized in the C-terminal half of the protein and is referred to as "activation function 2" (AF2). The extensive structural characterization of the ligand-binding domain of several receptors, such as estrogen receptor (ER) (2), progesterone receptor (PR) (2), and androgen receptor (3), has improved our understanding of the binding of the hormone, the resulting conformational changes in the receptor, and the basis of acute specificity of hormone binding to its receptor.

The DNA binding of ligand-activated NR represents the delivery of the signal to the genome, whereas further amplification of the signal is brought about by the ability of NRs to recruit a family of proteins broadly referred to as "coactivators." One of

* This work was supported in part by National Institutes of Health Grants CA98823 and CA65746 (to R. K.). The costs of publication of this article were defrayed in part by the payment of page charges. This article must therefore be hereby marked "*advertisement*" in accordance with 18 U.S.C. Section 1734 solely to indicate this fact.

[1] Both authors contributed equally to this work.

[2] Supported by a pre-doctoral fellowship from the W. M. Keck Foundation of the Gulf Coast Consortia through the Keck Center for Computational and Structural Biology.

[3] Support by the Robert A. Welch Foundation (Grant JM Q-1512).

[4] To whom correspondence should be addressed: Dept. of Molecular and Cellular Oncology, University of Texas M.D. Anderson Cancer Center, 1515 Holcomb St., Houston, TX 77030. Tel.: 713-745-3558; Fax: 713-745-3792; E-mail: rkumar@mdanderson.org.

[5] The abbreviations used are: NR, nuclear receptor; MTA1s, metastasis tumor-associated 1 short form; PELP1, proline-, glutamic acid-, and leucine-rich protein 1; E_2, estrogen (17-β-estradiol); ERα, estrogen receptor α; TFE, trifluoroethanol; ERE, estrogen response element; PR, progesterone receptor; NOESY, nuclear Overhauser effect spectroscopy; TOCSY, total correlation spectroscopy; dqf-COSY, double-quantum-filtered correlation spectroscopy; GST, glutathione *S*-transferase; AIB1 amplified in breast cancer-1.

the functions of coactivator proteins is to directly or indirectly remodel the local chromatin structure through covalent modification of histones (acetylation, phosphorylation, or methylation), resulting in the opening of chromatin, greater accessibility of the target gene promoter to transcription machinery, and ultimately, gene transcription (4). Numerous families of NR coactivators have been identified. The best studied include p300/CBP (CREB-binding protein), p300/CBP-associated factor, members of the SRC family (5), and proline, glutamic acid, and leucine-rich protein 1 (PELP1) (6).

Coactivator proteins have multiple signature motifs referred to as NR-boxes, which are short stretches of leucine-rich sequences with consensus sequence of L*XX*LL (where *X* denotes any amino acid residue). The binding of the cognate ligand to the ligand-binding domain of the NR results in a conformational change involving the rearrangement of the positions of helices H3, H4, H5, and H12, leading to the formation of a hydrophobic pocket. The NR-boxes bind to this hydrophobic pocket in a helical conformation with a high degree of affinity, thus leading to the recruitment of coactivators to the activated NR. The interaction of a NR with a specific coactivator is determined by the specificity of the binding interactions between the NR-box motif and the ligand-binding domain of the NR. In general, each coactivator has more than one NR-box, and the differences in spacing of the NR-boxes, combined with the variable flanking sequences, have been implicated in conferring the specificity of this interaction (7, 8).

Estrogen receptor α (ERα) belongs to a subfamily of NRs, namely steroid hormone receptors. It functions as an estrogen-activated transcription factor and is involved in the up-regulation of downstream target genes, most of which are involved in the control of cell cycle progression and growth of human breast epithelium. Excessive stimulation of the ER pathway in the cell due to increased hormonal secretion or increased activation of the receptor can lead to augmentation of cell proliferation and thus a higher risk of growth deregulation, possibly resulting in breast cancer (4). In this context, the mode of action of ERα, its potential deregulation in cancer, and its coregulatory protein are subjects of intense study.

In a previous report from this laboratory, we identified and characterized a unique coregulatory protein of ERα, namely MTA1s, which is a naturally occurring splice variant of MTA1 (9). MTA1s localizes in the cytoplasm, and its C-terminal stretch of 33 amino acids bears no resemblance to any of the previously reported protein sequences. Situated in the early portion of this 33-amino acid region is an NR-box motif bearing the sequence -LRILL- (Fig. 1*A*). MTA1s uses this motif to interact and bind with the AF2 domain of ERα, leading to its cytoplasmic sequestration, decrease in the genomic functions of ERα, and augmentation of the aggressive ER-negative phenotypes in cells like increased metastasis, invasiveness, and resistance to antiestrogen therapy. In the present investigation, we elucidated the NMR solution structure of this stretch of 33 amino acids of MTA1s. Then, in an *in silico* modeling study, we simulated the binding of the NR-box motif to the AF2 domain of ERα. We determined the effects of MTA1s peptide on ERα transactivation function, estrogen-stimulated proliferation, and tumorigenesis of breast cancer cells.

MATERIALS AND METHODS

Cell Culture and Reagents—Human breast cancer cells were cultured in Dulbecco's modified Eagle's medium/F-12 medium supplemented with 10% fetal bovine serum. For estrogen treatment experiments, the regular medium was replaced with medium containing 5% dextran-charcoal-stripped medium. The C-terminal 33-amino acid peptide of MTA1s was purchased from SynPep Corp. (Dublin, CA) and fully characterized by reverse phase high-performance liquid chromatography, amino acid sequencing, and mass spectrometry.

Far-UV Circular Dichroism Spectroscopy—Far UV CD spectra of the peptide dissolved in different concentrations of trifluoroethanol (TFE) (30, 40, 50, and 70%) were recorded from 260 to 210 nm using a JASCO J-810 spectropolarimeter using 0.1-cm quartz cuvettes. Each spectrum was an average of five scans.

NMR Spectroscopy—Perdeuterated TFE was supplied by Cambridge Isotope Inc. NMR samples were prepared by dissolving 4 mg of MTA1s peptide in 550 μl of a 1:1 mixture of perdeuterated TFE and H_2O or perdeuterated TFE and 99.96% D_2O. Proton NMR spectra were recorded either on a Varian UnityPlus spectrometer (Palo Alto, CA) operating at 750 MHz or a Bruker Avance (Billerica, MA) spectrometer operating at 500 MHz equipped with $^{1}H/^{13}C/^{15}N$ triple resonance probes with pulse-field gradients. All experiments were performed at 25 °C, and the water peak was suppressed using either WET (10, 11) or WATERGATE (12) solvent suppression sequences. Two-dimensional Nuclear Overhauser effect spectroscopy NOESY, total correlation spectroscopy (TOCSY), and double-quantum-filtered correlation spectroscopy (dqf-COSY) spectra were collected with the states-time proportional phase increment method. Double-quantum-filtered two-dimensional correlation (13) spectra were collected with 4096 points in the t_2 dimension, 400 real t_1 increments, 32 transients per free induction decay, and a 2-s recycle delay. The data were zero-filled to 1024 points in the t_1 dimension and multiplied by a 20°-shifted sine bell function in both dimensions prior to Fourier transformation. Estimates of NH-CαH coupling constants ($^{3}J_{NH}$) were obtained from the peak separation of multiplets in the dqf-COSY spectrum. TOCSY spectra (14) were recorded at mixing times of 30, 60, and 75 ms with 4096 data points in the t_2 dimension and 320 t_1 increments. NOESY spectra (15) were collected with 4096 data points in the t_2 dimension and 320 real t_1 increments using the states-time proportional phase increment method of phase cycling. Thirty-two transients per free induction decay were collected, with a relaxation delay time of 3.5 s. Mixing times of 60, 180, 250, and 400 ms were used. All NOESY spectra were zero-filled to 2048 in the t_1 dimension prior to Fourier transformation and apodized with a 90°-shifted sine bell function. A NOESY spectrum with a 400-min mixing time was used only for resonance assignments. All spectra were processed on an SGI workstation using Felix version 2000 (Accelrys, Inc., San Diego, CA) and internally referenced to the residual CDH resonance of perdeuterated TFE (3.9 ppm).

Structure Calculations—Inter-proton distances were estimated from NOESY cross-peak intensities using Felix. NOESY intensities were classified as strong, medium, weak, or very

weak and were assigned distance ranges of 1.8–2.5, 1.8–3.5, 1.8–4.5, or 1.8–5.5 Å, respectively, to be used as distance restraints in molecular dynamics simulation with XPLOR 3.1 (16). This produced a total of 310 inter-proton distance constraints. A linear peptide chain of the sequence was generated using XPLOR and was subjected to 10 ps of unrestrained molecular dynamics in the absence of any Van der Waal repulsion to generate a family of 30 initial randomized structures. Each of these structures was subjected to 500 steps of restrained energy minimization using the steepest descent algorithm and subsequently subjected to restrained molecular dynamics. The restrained molecular dynamics protocol consisted of 10 ps of restrained molecular dynamics at 1000 K, during which the Van der Waals' force constant was gradually increased. Each structure was subjected to an additional 5 ps of molecular dynamics at the maximum Van der Waals' force constant and was followed by a cooling step to 300 K over 7 ps. Finally, each structure was subjected to 1000 steps of energy minimization. A final 20 structures with the lowest energies and the least NOE violations were retained for structural analysis. The progress of structure refinement was visually monitored using the molecular modeling program Insight II (2000) (Accelrys, Inc.).

Glutathione S-Transferase Pulldown Assay—In vitro transcription and translation of proteins was performed using a T7-TnT kit (Promega), where 1 μg of cDNA in pcDNA 3.1 vector was translated in the presence of [^{35}S]methionine (for full-length ERα) and unlabeled, cold methionine (for the PELP1 N-terminal 1- to 400-amino acid region) in a reaction volume of 50 μl. The reaction mixture was diluted to 1 ml with Nonidet P-40 lysis buffer (25 mM Tris, 50 mM NaCl, and 1% Nonidet P-40). An equal aliquot was used for each GST pulldown assay. Translation and product size were verified by subjecting 5% of the reaction mixture to and autoradiography. The GST pulldown assays were performed by incubating equal amounts of the GST-tagged C-terminal 33-amino acid region of MTA1s, immobilized on glutathione-Sepharose beads (Amersham Biosciences) with the *in vitro*-translated ^{35}S-labeled protein whose binding was being tested. Bound proteins were isolated by incubating the mixture for 3 h at 4 °C, after which the proteins were washed five times with Nonidet P-40 lysis buffer, eluted with 2× SDS buffer, and separated by SDS-PAGE. The bound proteins were then visualized by fluorography.

Immunofluorescence and Confocal Microscopy Studies—We determined the cellular localization of proteins by indirect immunofluorescence. In brief, cells grown on glass coverslips were fixed in 4% phosphate-buffered paraformaldehyde for 15 min. Cells were permeabilized in methanol at −20 °C for 4 min. Cells were then incubated with primary antibodies for 2 h at ambient temperature, washed three times in phosphate-buffered saline, and incubated with secondary antibodies conjugated with 546-Alexa (red) or 488-Alexa (green) from Molecular Probes (Eugene, OR). The DNA dye Topro-3 (Molecular Probes) was used to co-stain the DNA (blue). Confocal scanning analysis was performed with an Olympus FV300 laser scanning confocal microscope in accordance with established methods, using sequential laser excitation to minimize the possibility of fluorescent emission bleed-through. Each image is a three-dimensional reconstructed image of stacks of serial Z sections at the same cellular level and magnification. Co-localization of two proteins is shown as *yellow* for red and green fluorescence.

Liposomal Encapsulation of the Peptide—A liposomal formulation of a 33-amino acid peptide was prepared as follows. Ten milliliters of *t*-butanol was added to 10 mg MTA1s peptide. Ddimyristoylphosphatidylcholine (Aventi Lipids, Alabaster, AL) was added to *t*-butanol (125 mg of dimyristoylphosphatidylcholine:25 ml of *t*-butanol). After lipid was dissolved, Tween 20 (187 μl) was added to the lipid solution. The peptide and lipid solutions were then combined and mixed. After freezing the solution was lyophilized for 24 h. The resulting white powder was dissolved by addition of saline, and the contents were shaken by hand for 5 min. This process was repeated in a separate sample with addition of no peptide and was considered as control liposome.

Transfection and Promoter Assays—Cells were maintained in Dulbecco's modified Eagle's medium/F-12 (1:1) supplemented with 10% fetal calf serum. For reporter assays, the required plasmids were transiently transfected using the FuGENE 6 kit from Roche Applied Science as per the manufacturer's instructions. Cells were cotransfected with β-galactosidase, and a luciferase assay was performed using the Luc assay kit (Promega).

Reverse Transcription-PCR Analysis—Reverse transcription-PCR was performed using the Access RT-PCR kit (Promega) and specific primers for c-*myc*, total PR, and actin; the sequence details are as follows: PR, CAAATGAAAGCCAAGCCCTA and TGCCTCTCGCCTAGTTGATT; *c-myc*, CTCCTGGCAAAAGGTCAGAG and AGCTTTTGCTCCTCTGCTTG; and actin, GGACTTCGAGCAAGAGATGG and ACATCTGCTGGAAGGTGGAC.

Cell Proliferation, Soft Agar, and Tumorigenesis Assays—For cell proliferation assays, cells were grown in phenol red-free medium supplemented with 5% dextran-charcoal-stripped serum for 48 h and then treated with estrogen. The proliferation rate of the cells was measured by counting them in a Beckman Coulter Counter as previously described (17). Soft-agar colony-growth assays were performed as previously described (18). In brief, 1 ml of 0.6% Difco agar in Dulbecco's modified Eagle's medium supplemented with 5% dextran-charcoal-stripped serum and insulin was layered onto tissue culture plates. Test cells (1×10^4) mixed with 1 ml of 0.36% Bacto agar solution in Dulbecco's modified Eagle's medium were layered on top of the 0.6% Bacto agar layer. The plates were incubated at 37 °C in 5% CO_2 for 21 days. For tumorigenesis studies, 5×10^7 cells were implanted into the mammary fat pads of six nude mice as previously described (19). Female athymic mice, 4–6 weeks of age (NCI, National Institutes of Health, Frederick, MD) were housed in sterile environmental condition. All animal procedures were performed in compliance with the Institute Animal Care and Use Committee and National Institutes of Health Policy on Humane Care and Use of Laboratory Animals.

RESULTS

Far-UV CD Analysis of MTA1s Peptide—The 33-amino acid peptide had a high degree of hydrophobicity because of an abundance of hydrophobic amino acids (five leucines, three

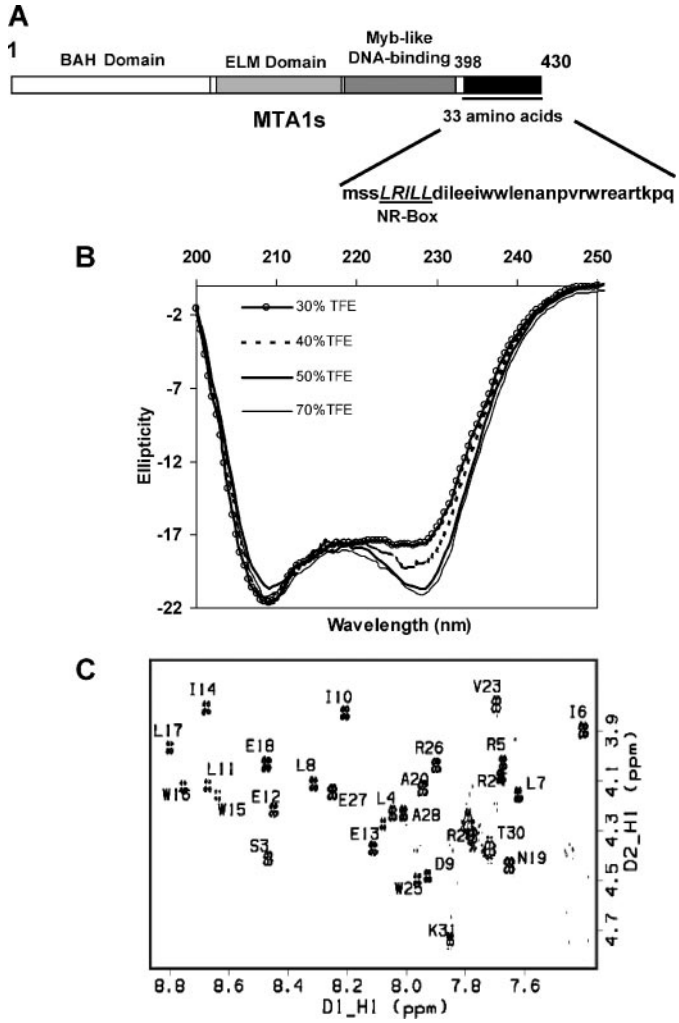

FIGURE 1. **Far-UV CD and dqf-COSY spectrum of MTA1s C-terminal 33-amino acid peptide region.** *A*, schematic representation of different structural domains of MTA1s and the sequence of the C-terminal 33-amino acid region. The NR-box motif is highlighted. *B*, far-UV CD spectra of the 33-amino acid C-terminal peptide of MTA1s dissolved in different concentrations of TFE in water were recorded between 260 and 200 nm. Characteristic spectra of predominantly α-helical region are observed at all concentrations of TFE. *C*, NH-CαH correlations in the dqf-COSY spectrum acquired at 750 MHz in 50% TFE/50% H_2O, pH 4.7, at 25 °C. Cross-peaks are labeled according to residue.

tryptophans, three isoleucines, one valine, and one methionine) and consequently had low solubility in the complete aqueous system. The presence of TFE at 30% or more in solution facilitated the dissolution of the peptide. To gain preliminary insight into the solution structure of the peptide, we initially performed a far-UV CD spectral analysis with different percentages of TFE in sterile Millipore water (Fig. 1*B*). The spectra showed the two characteristic peaks at 208 nm and 225–230 nm at all concentrations of TFE and showed the predominance of the α-helical structure. A noticeable increase in ellipticity between 225 and 230 nm was observed among the samples in 30%, 40%, and 50% TFE there were no further structural changes when the TFE concentration was increased beyond 50%.

NMR Spectral Assignment—Solubility of the peptide in water was not sufficient to create a sample with the concentrations required for NMR studies. As the solubility could be increased with the addition of TFE, the NMR experiments were performed in a mix solvent of TFE and H_2O. Because there was evidence of multiple conformations at lower TFE:H_2O ratios, we collected a series of TOCSY spectra at TFE:H_2O ratios of 30:70%, 50:50%, and 70:30% to determine the optimum solvent conditions for NMR studies. The multiple peaks present at lower TFE:H_2O ratios disappeared at the 50:50% solvent ratio, and the spectra underwent no further substantial changes when the TFE:H_2O ratio was increased to 70:30%. This observation was consistent with the CD data collected at increasing TFE:H_2O ratios, and all NMR spectra were collected with samples made in TFE/H_2O mixture (1:1) at ambient temperature and pH 4.7.

Proton resonance assignment was accomplished using the standard sequential resonance assignment method outlined by Wuthrich (20); with it, we identified the proton spin systems of all amino acids using dqf-COSY and TOCSY spectra followed by the establishment of sequential NH-CαH, NH-CβH, and NH-NH correlations using NOESY spectra. The dqf-COSY spectrum produced 27 well resolved correlations of 31 possible NH-CαH cross-peaks in its fingerprint region (Fig. 1*C*). Three of the missing four correlations could be observed in the corresponding region of the TOCSY spectrum. By combining the spin-system information obtained from the scalar experiments with the through-space correlations in NOESY spectra, tryptophans 15 and 16 were used as the starting point in tracing the sequential connectivity patterns.

NMR data strongly suggested the existence of the N-terminal helical region and the two turn structures toward the C terminus, but we found no evidence of a long-range interaction between the helical and C-terminal regions to suggest any stable tertiary fold in the molecule. In fact, the less orderly regions between the structured regions of the molecule rendered the C-terminal more flexible. CαH resonances of the residues in the C terminus also displayed significant chemical shift deviations from their standard random coil values, which suggested a regular helical geometry similar to the N terminus. However, there were not enough medium range NOE interactions that are typical of continuous helical structures.

Structure Refinement—The three-dimensional structure calculation was performed with 310 inter-proton distances (174 inter-residue and 136 intra-residue) using the simulated annealing protocol within XPLOR 3.1. The overlay of the 12 structures is shown in Fig. 2*A*, and the stereo view of the energy-minimized mean structure of the 12 final structures is shown in Fig. 2*B*. Residues Met-1 through Ser-3 were largely unstructured in all final structures. As the mean structure shows, there was a stable helical region from Leu-4 through Leu-17 with a loosely defined helical segment from Leu-7 through Asp-9. The helical segment spanning the first three residues displays the characteristics of the 3–10 helix, whereas the remainder of the helix (Ile-10 through Leu-17) represents a regular α-helix. Because of the stable structure in the N-terminal region of the molecule, more than 60% of the extracted structural restraints came from the Ser-3 through Glu-18 segment. The smaller number of restraints per residue in the region immediately following the α-helix provides increased flexibility to the C-terminal region (Table 1).

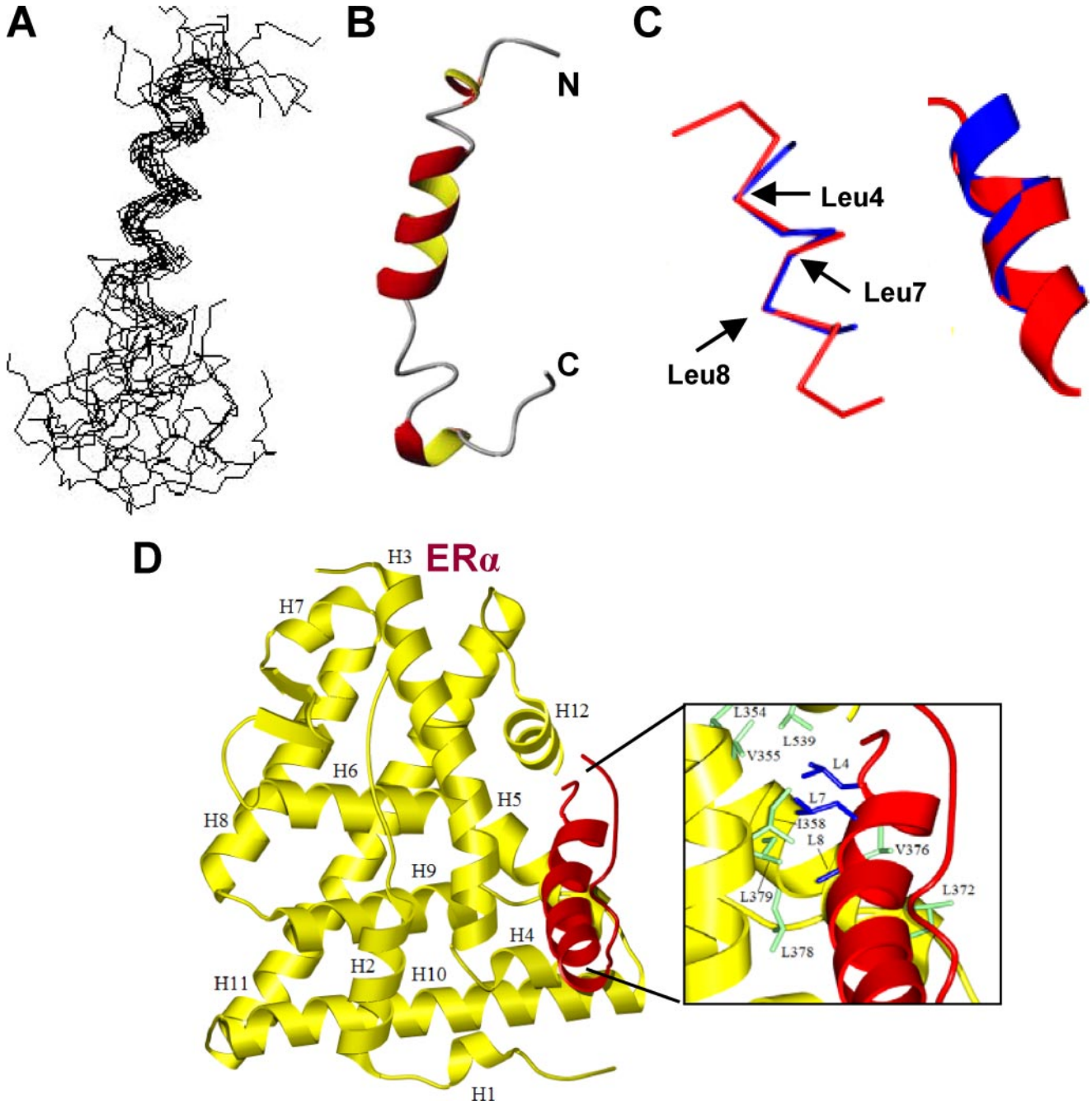

FIGURE 2. **Detailed solution structure of the MTA1s peptide derived by NMR spectroscopy and *in silico* docking studies of the peptide with AF2 domain of ERα.** *A*, overlay of the family of 12 final structures of MTA1s peptide. *B*, stereoview of the mean structure of the family of 12 final structures. *C*, rigid-body superimposition of the NR-box motif of MTA1s peptide (*red*) to that of the TIF2 NR-box2 (*blue*) shows a high degree of structural similarity with the root-mean-square difference being 0.09 Å. The positions of the leucine residues of the MTA1s NR-box (Leu-4, Leu-7, and Leu-8) are indicated. The *ribbon diagram* also shows the structural similarity of the motifs. *D*, the structure of the NR-box motif of the MTA1s peptide derived from the NMR data was docked *in silico* with the AF2 domain of ERα derived from the x-ray crystallographic studies (PDB code 1GWQ).

In Silico Comparison and Docking of the NR-box Region of the MTA1s Peptide Shows Potential Similarity of Interaction with NR-box Motif of Co-regulators—To compare the similarity of this NR-box to the NR-box of the coactivators, the positions of Cα atoms of leucines 4, 7, and 8 of the MTA1s peptide were overlapped with the three Cα atoms of the leucines in the NR-box2 motif of the coactivator TIF2/SRC2/NCoA2 (21) (PDB code 1GWQ). A rigid-body superimposition of the -LRILL- motif of the MTA1s peptide was done by placing the NR-box motif of TIF2 over the x-ray structure of 1GWQ. A high degree of structural overlapping was observed between the NR-box of MTA1s peptide and the NR-box2 of TIF2, which is indicated by a root-mean-square difference of 0.09 Å, clearly evident from the backbone overlapping and ribbon diagrams of the two motifs (Fig. 2*C*). *In silico* docking of the MTA1s peptide structure (as determined from the NMR study) was performed on the leucine-rich, NR-box-binding hydrophobic pocket of the ERα AF2 domain, the structure of which was taken from the previously derived x-ray crystallographic structure (21). The docking studies revealed that leucines 4, 7, and 8 of the -LRILL-

TABLE 1

Summary of input restraint for MD calculations and structural statistics of the final structure

The parameters are given for the average structure of ensemble of 20 lowest energy structures. There were no NOE violations >0.2 Å or dihedral angle restraint violations of >5°.

Inter proton distance restraints	
Intra-residue	136
Sequential	113
Medium range	61
Total	310
Root-mean-square deviation from ideal geometry	
Bond lengths (Å)	0.021
Bond angles (°)	2.4
Ramachandran plot analysis	
Residues in most favorable regions (%)	62.1
Residues in additional allowed regions (%)	17.2
Residues in generously allowed regions (%)	13.8
Residues in disallowed regions (%)	6.9
Root-mean-square deviation (residues 4–16 to the mean)	
Backbone (Å)	1.01
Heavy atoms (Å)	1.67

motif of the MTA1s peptide could interact with Leu-354, Val-355, and Ile-358; Leu-372, Val-376, Leu-378, and Leu-379; and Leu-539, Leu-540, Leu-541, and Leu-544 of the ERα AF2 domain, respectively (Fig. 2*D*, enlarged in the *inset*). These studies showed the potential similarity of the NR-box motif of the MTA1s peptide to the similar motif of a coregulator and explained the strong binding ability of the MTA1s 33-amino acid region to ERα.

Overexpression of MTA1s Peptide Represses ERα Transactivation Function—The C-terminal 33-amino acid region of MTA1s has a unique sequence and an NR-box motif (-LRILL-) that interacts strongly with the AF2 domain of ERα. MTA1s mutant with the 33-amino acid region or NR-box motif deleted was incapable of binding to ERα and sequestering it in the cytoplasm losing its efficacy as an inhibitor of ERα transactivation functions (9).

Next, we determined the effect of the 33-amino acid peptide on the ERα nuclear functions by an ERE-luc assay, with transient overexpression of the T7-tagged peptide in MCF-7 cells. A drastic repression of ERα was observed, in the ERE-luc assay both in the presence and absence of estrogen (Fig. 3*A*). The repression caused by overexpression of full-length MTA1s was used as a positive control. Overexpression of the T7-tagged peptide in the MCF-7 cells was shown by confocal immunofluorescence microscopy (Fig. 3*A*, *inset*).

In a similar experiment, different concentrations of the tagged peptide were transiently expressed in MCF-7 cells, and ERα transactivation functions were repressed in a dose-dependent manner (Fig. 3*B*). In another assay, MCF-7 cells were treated with two different doses of liposome-encapsulated, biotin-labeled peptide, and an ERE-luc assay was performed. At a peptide concentration of 1 μg/ml, a substantial repression of ER transactivation was observed, and this effect was further enhanced at the concentration of 5 μg/ml (Fig. 3*C*). The successful delivery of the biotin-labeled peptide into the cells was evident by streptavidin staining of the cells, which is shown in the figure *inset* along with cells treated with control empty liposomes for comparison. In brief, we found that the 33-amino acid region of MTA1s strongly repressed ERα transactivation functions.

MTA1s 33-Amino Acid Region Binds to ERα, Competes for Binding Sites with Coregulators, and Negatively Regulates ERα Target Genes—In cells, MTA1s is localized to the cytoplasm and functions as a repressor of ERα transactivation by binding and sequestering it in the cytoplasm. The strong repression of ER transactivation by the 33-amino acid peptide, which was localized in both the cytoplasm and the nucleus (as evident by the staining shown in Fig. 3), indicated that the MTA1s 33-amino acid peptide acts as a repressor of ER through a mechanism different from that employed by the full-length MTA1s.

As mentioned earlier, deletion of the NR-box motif present in the 33-amino acid region resulted in MTA1s losing its ability to bind and inhibit ERα (9). Comparison studies showed that the NR box of the MTA1s peptide had similar potential to interact with the AF2 domain of ERα (Fig. 2*D*), which raised the possibility that the peptide inhibits ERα by binding to the AF2 domain and potentially competes for binding sites with the coactivator proteins.

To explore this possibility, we next performed an ER transactivation assay in MCF-7 cells and evaluated the effect of the MTA1s peptide on the stimulation of ERα transactivation function by AIB1, a coactivator belonging to the p160 family. Transient overexpression of AIB1 in MCF-7 cells stimulated ERα activity by >2-fold (Fig. 4*A*). Transient expression of Myc-tagged MTA1s peptide, along with overexpression of AIB1, blocked the effect of AIB1 and resulted in a dose-dependent repression of ERE-luc activity (Fig. 4*A*), suggesting that the MTA1s peptide may antagonize the effect of AIB1 by competing with it for binding sites on ERα. This hypothesis was further supported by *in vitro* binding studies, where the binding of the GST-tagged MTA1s 33-amino acid peptide to ERα was competed out by the NR-box-rich region of the recently characterized coactivator of ER, PELP1.

PELP1 was initially identified as a novel coactivator of ERα and found to be a powerful potentiator of ERα transactivation functions. PELP1 has a total of nine NR-box motifs, seven of which are present in the N-terminal 400-amino acid region (6). The GST-tagged MTA1s 33-amino acid peptide showed strong binding to full-length *in vitro*-translated ^{35}S-labeled-ERα (Fig. 4*B*). This binding could be competed out by introducing the *in vitro*-translated, unlabeled, NR-box-rich, 1- to 400-amino acid N-terminal region of PELP1. The presence of the PELP1 N-terminal region blocked the binding of the GST-tagged MTA1s peptide to ERα (Fig. 4*B*). The direct *in vitro* effect of the peptide on the binding of coactivators to ERα could not be tested because of the low solubility of the peptide in solution, as mentioned earlier. In the *in vitro* binding study, the binding of GST-tagged MTA1s to ERα was abrogated by the presence of the PELP1 NR-box-rich region, which indicated the mutual competition of the MTA1s peptide with the NR-box motifs of the coregulator for the binding site.

The repressive effect of MTA1s peptide on the transactivation activity of ERα was further evidenced by the effect of the peptide on the transcription of ERα target genes. The expression of two target genes, c-*myc* and *PR* was examined in MCF-7 cells (Fig. 4*C*). Cells were treated with liposome-encapsulated MTA1s peptide (2.5 μg/ml) or empty liposomes for 2 days prior to estrogen treatment. Total RNA was extracted, and the status

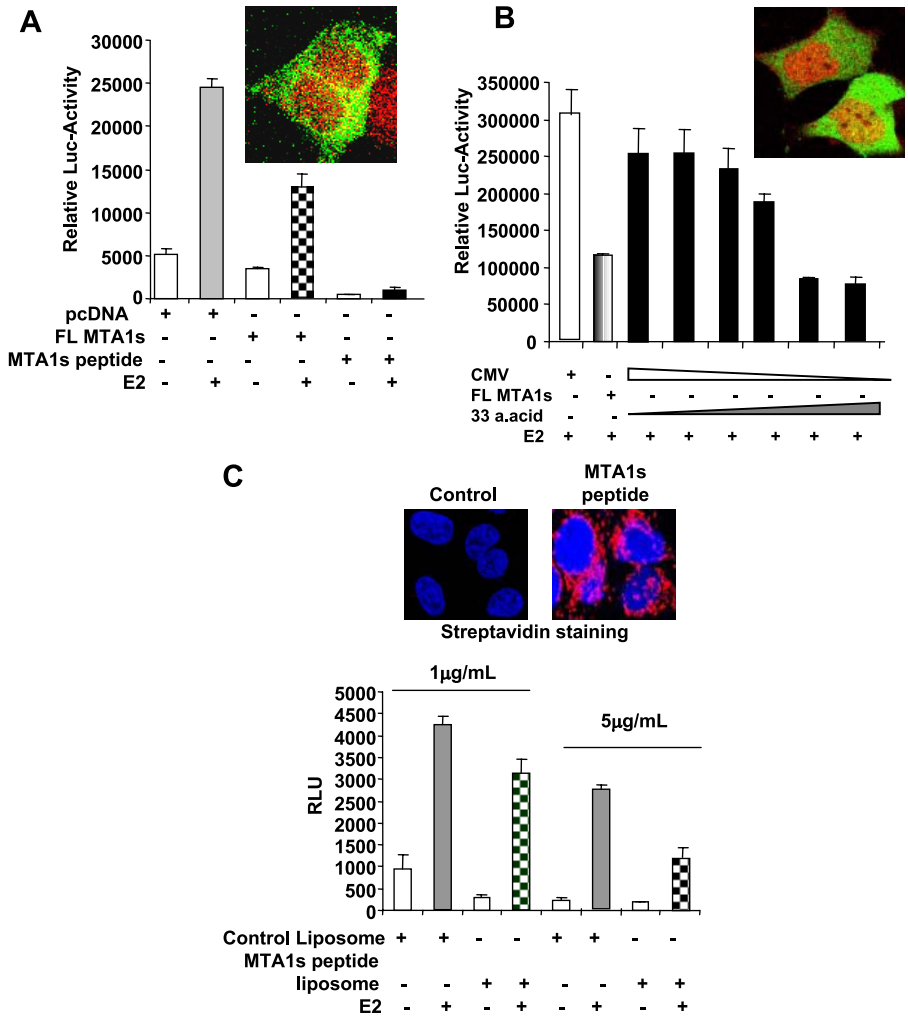

FIGURE 3. **Overexpression of MTA1s peptide or delivery by a liposome system represses ERα transactivation functions in breast cancer cells.** *A*, T7-tagged MTA1s C-terminal 33-amino acid peptide was transiently overexpressed in MCF-7 breast cancer cells, and an ERE-luc assay was done. Drastic repression of the luc activity was observed both under basal and estrogen-stimulated conditions. Repression of the ERE-luc activity by full-length MTA1s was used as positive control and for comparison to highlight the ERα repressing ability of MTA1s peptide. The efficient expression of the peptide in the cells is shown by confocal microscopy where staining was with anti-T7 tag antibody (*inset*). *B*, dose-dependent repression of estrogen-stimulated ERE-luc assay by transient expression of increasing amounts of Myc-tagged MTA1s peptide in MCF-7 cells. Increasing amounts of expression plasmid DNA (100 ng, 200 ng, 400 ng, 600 ng, 800 ng, and 1 μg) for Myc-MTA1s peptide were transfected. Expression of the peptide is shown by confocal microscopy with anti-Myc antibody staining (*inset*). *C*, MCF-7 cells were treated for 48 h with either empty liposomes or liposomes with biotin-labeled MTA1s peptide, after which an ERE-luc assay was done. Dose-dependent repression of the luc activity was observed at two different concentrations of peptide delivery (1 μg and 5 μg of peptide/ml of culture media) demonstrating the repressive action of the MTA1s peptide on ERα transactivation functions. Efficient delivery of the biotin-labeled peptide into the cells is shown by confocal microscopy with streptavidin-tagged antibody (*inset*). The concentration of E_2 used in all the above experiments was 10^{-9} M.

of c-*myc* and *PR* was evaluated by RT-PCR. A clear induction of c-*myc* and *PR* expression was evident in the control cells; however, treatment with MTA1s peptide reduced both the basal and estrogen-induced up-regulation of these two genes, suggesting a negative regulatory effect of the MTA1s peptide on the ERα pathway (Fig. 4*C*).

MTA1s Peptide Inhibits Estrogen-induced Proliferation and Anchorage-independent Growth in Cells—Estrogen is a strong inducer of mammary epithelial cell proliferation. The inhibitory effects of the MTA1s peptide on ERα transactivation functions and target gene expression prompted us to study its effect on estrogen-induced cell growth in MCF-7 cells. Cells were treated with liposome-encapsulated MTA1s peptide for 2 days, after which they were stimulated with estrogen and the extent of proliferation was measured by estimating the cell number. Cells treated with empty liposomes were used as the control. We found that, as expected, estrogen treatment stimulated cell growth, with a maximum effect after 3 days of treatment (Fig. 5*A*). The noted stimulation of cell proliferation by estrogen was considerably inhibited by the MTA1s peptide. In fact, the growth rate of these cells was comparable to or even lower than that of estrogen-starved cells (Fig. 5*A*). These findings suggest that the MTA1s peptide acts as a potent inhibitor of estrogen-induced cell proliferation. We next determined the effect of the MTA1s peptide on the estrogen-induced, anchorage-independent growth of MCF-7 cells. The colony formation ability of MCF-7 cells was assayed in the presence or absence of MTA1s peptide. As expected, estrogen stimulated anchorage-independent growth by 5-fold (Fig. 5*B*). Under similar conditions, in the cells treated with the MTA1s peptide, the estrogen-induced anchorage-independent growth was substantially decreased. The size of colonies was also in the peptide-treated cells were drastically reduced in comparison with the size of control cell colonies (Fig. 5*B*, *inset*). Together, these studies suggest that the MTA1s peptide effectively inhibits the biological effects of estrogen, which may be due to its inhibitory effect on ER transactivation activity.

MTA1s Peptide Inhibits Tumorigenesis Induced by Overexpression of the Coactivator PELP1—PELP1-overexpressing MCF-7 cells have been shown to efficiently form tumors in nude mice (22). Therefore, to further establish the inhibitory activity of the MTA1s peptide on cell proliferation, we tested its ability to interfere with PELP1-induced tumorigenesis by injecting the mammary fat pads of six nude mice with PELP1-overexpressing cells. After 4 weeks, liposomes with or without biotin-labeled MTA1s peptide were injected into the tumors. The tumor progression was determined by measuring the tumor size every week for the next 2 weeks. The percentage changes in the tumor volume (increase or decrease) in each mouse (mean of two tumors, one in each flank) were calculated and are shown in Fig.

6. Mice not treated with MTA1s peptide showed a continuing trend of tumor growth in the first week, but no further growth was observed in the second week. In mice injected with the MTA1s peptide, the growth of tumors in the first week was noticeably lower than that in the control group, and in the second week, there was a drastic decrease in tumor size, indicating that the peptide blocked tumor growth (Fig. 6). Streptavidin staining for biotin showed evidence of efficient delivery of the biotin-labeled MTA1s peptide into the tumor, which was distinctly absent from the tumors injected with the control liposomes (Fig. 6).

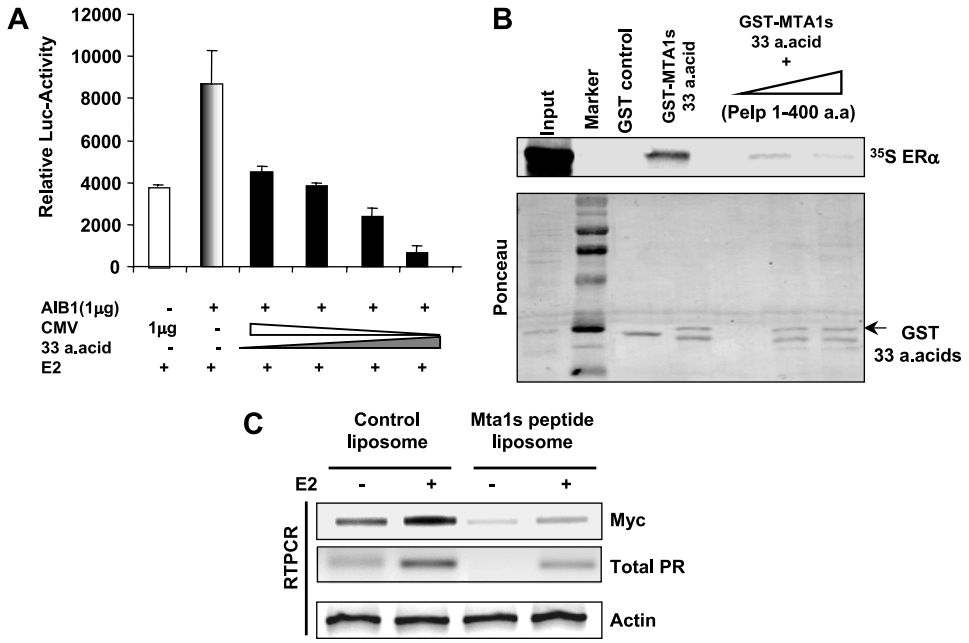

FIGURE 4. **MTA1s peptide antagonizes the stimulation of ERα functions by coactivator AIB1 and represses the expression of ER target genes.** *A*, ERE-luc assay was done in MCF-7 where the effect of different amounts of transiently expressed Myc-tagged MTA1s peptide on the ability of the coactivator AIB1 to stimulate ERα transactivation function. Increasing amounts of expression plasmid DNA (250 ng, 500 ng, 750 ng, and 1 μg) for Myc-MTA1s peptide expression vector plasmid were transfected. Dose-dependent repression of the luc activity was observed with increasing expression of the MTA1s peptide despite overexpression of AIB1 indicating the ability of the peptide to antagonize the stimulatory functions of AIB1. *B*, the *in vitro* binding of the GST-tagged MTA1s 33-amino acid region to ^{35}S-labeled ERα was competed out by excess of the *in vitro*-translated, 1- to 400-amino acid, NR-box-rich region of ERα coactivator PELP1 showing the mutual competition of the NR-box motif of MTA1s peptide and the NR-box motifs of the coactivator. *C*, The effect of the MTA1s peptide on the expression levels of estrogen regulated-genes like c-Myc and total *PR* in MCF-7 cells was tested by reverse transcription-PCR analysis. Cells were treated with empty liposomes and liposomes with MTA1s peptide (2.5 μg/ml) for 48 h under estrogen starvation after which they were stimulated with estrogen (10^{-9} M) for 16 h followed by extraction of total RNA and reverse transcription-PCR for the target genes. Considerable repression of expression of c-*myc* and *PR* was observed with peptide treatment in comparison to the control cells, under both the basal and estrogen treatment. Expression of actin was used as control across samples and is shown below. The concentration of E_2 used was 10^{-9} M.

DISCUSSION

The functions of ERα at the molecular level are modulated by the activity of two major functional domains, AF1 and AF2 (23, 24). AF1 comprises the N-terminal portion and has specific sites that are subjected to covalent modifications such as phosphorylation, acetylation, ubiquitination, and palmitoylation (4). AF2 is situated toward the C-terminal end and is involved in the activation and repression of the ERα transactivation function. The binding of estrogen to the ligand-binding pocket results in the formation of a hydrophobic groove by helices 3, 4, 5, and 12 (25). This groove functions as the docking site for NR-box motifs of the coactivators, which forms a general basis for the recruitment of coactivators to NRs, ultimately leading to chromatin modification and gene transcription (26). The NR-box core motif (-L*XX*LL-) of the coregulators, along with the N-terminal and C-terminal flanking residues, has enough information to interact with the NRs with a high degree of specificity (7).

Previously, we reported that MTA1s, a novel coregulatory protein of ERα, exploits the specificity of an NR-box motif in its C-terminal region, using it to bind to the AF2 domain of ERα and sequester it in the cytoplasm, thus inhibiting its nuclear functions (9). The present investigation represents a comprehensive structural and functional characterization of the unique C-terminal 33-amino acid sequence of MTA1s containing this NR-box motif.

Preliminary CD analysis of this peptide in various concentrations of TFE indicated a predominantly helical structure (Fig. 1*B*), which was confirmed by the detailed NMR spectroscopic analysis. The family of 12 final structures showed that residues Met-1 to Ser-3 are largely unstructured and have the features of a 3–10 helix. We found a α-helical secondary structure from the residue Ser-3 to Leu-17 (Fig. 2). The NR-box motif forms the earlier part of the N-terminal helical region. Beyond the helical region was a turn-like structure around Pro-22, which was found to be predominantly in trans-conformation. In total, the C-terminal region had two turn-like structures and exhibited greater structural flexibility (Fig. 2*A*) than did the N-terminal region. No tertiary structural elements were observed, which could be attributed to the lack of interactions between the helical N-terminal region and the flexible C-terminal region.

On *in silico* comparison, the NR-box motif of MTA1s and the NR-box2 motif of the well characterized coactivator SRC2/TIF2 showed a high degree of similarity, both in structure and in the ability to dock with the ligand-activated AF2 domain of ERα (Fig. 2, *C* and *D*). This similarity may be explained by the strong binding ability of the MTA1s NR-box motif to ERα and raises the possibility that this C-terminal 33-amino acid region can function as a competitor of coactivator binding to ERα, thus inhibiting the transactivation function of ERα. This was indeed found to be the case when we tested the effect of this peptide with an ERE-luc assay. Both transient overexpression of the peptide and delivery through the liposomal system in MCF-7 breast cancer cells led to efficient repression of ERα (Fig. 3), suggesting the antagonistic nature of the MTA1s 33-amino acid peptide.

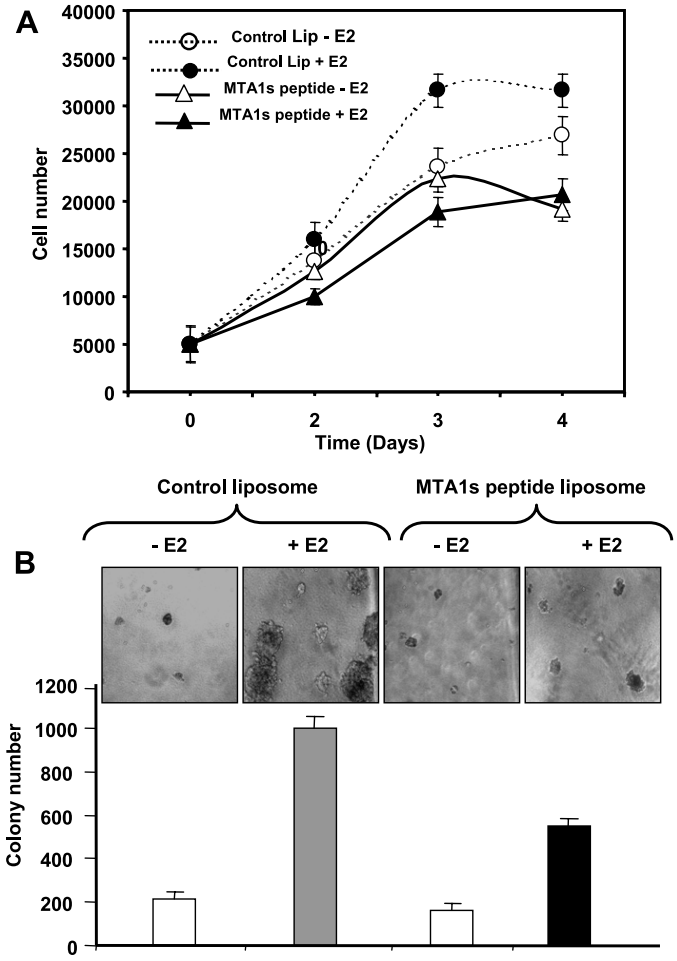

FIGURE 5. **MTA1s peptide inhibits estrogen-induced cell proliferation and anchorage-independent growth.** *A*, the estrogen-stimulated proliferation of MCF-7 cells treated with empty or MTA1s peptide liposomes (5 μg/ml peptide) was tested by estimating the total cell count every 24 h for 4 consecutive days. Under estrogen stimulation, a considerable decrease of proliferation rate was observed in cells treated with MTA1s peptide in comparison to the cells treated with empty liposomes showing down-regulation of cell proliferation on peptide treatment. Results shown are an average of two different experiments. *B*, effect of the MTA1s peptide (5 μg/ml) on the estrogen-induced anchorage-independent growth of MCF-7 cells was tested by soft agar assay. Colony numbers were counted after 3 weeks of growth. A considerable decrease of the colony size and number was observed in cells treated with the peptide. The quantitation of the colony number is shown below and is an average of five different fields from three independent plates for each condition.

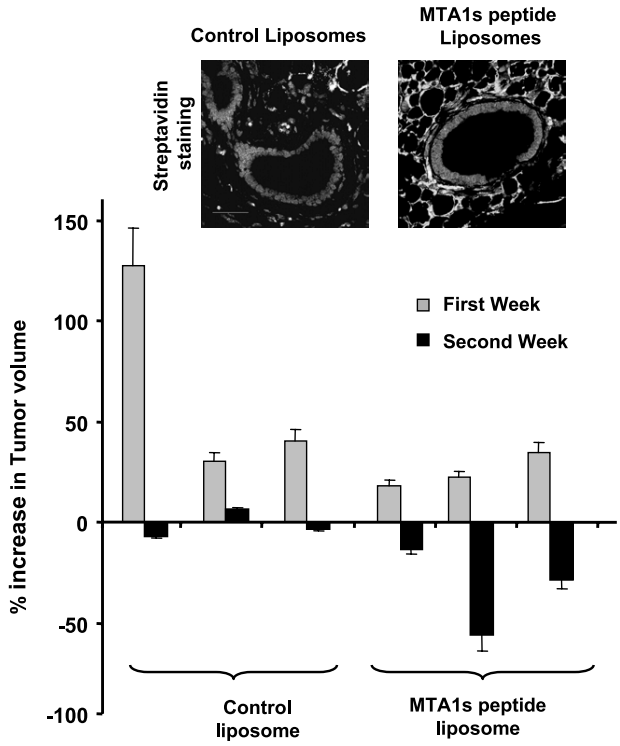

FIGURE 6. **MTA1s peptide inhibits PELP1-induced tumor growth in a xenograft assay.** PELP1-induced tumors were generated by xenograft in 6 female athymic mice by injecting PELP1-overexpressing MCF-7 cells into mammary fat pads. After 4 weeks of tumor growth the mice were divided into two groups of three each so as to get the same total tumor volumes in each group. Injections of MTA1s peptide liposome (40 μg of peptide/tumor) or empty liposomes were delivered directly into the tumors, and growth was followed for the next 2 weeks by measuring the tumor volume. The changes in average tumor volume from the two tumors in each mouse for the first and second week after the liposomal injections clearly show a down-regulation of the growth by the delivery of the MTA1s peptide into the tumors. Representative pictures of the tumor sections stained with streptavidin-tagged antibodies are shown above.

MTA1s was identified as a naturally occurring, alternatively spliced form of MTA1 (715 amino acids) that is smaller (430 amino acids) and lacks the nuclear localization signal observed in MTA1 (9). MTA1s represses ERα but does so via a different mechanism from the one used by MTA1 (27). In MTA1s, repression occurs through the binding and sequestration of ERα in the cytoplasm, preventing its ligand-induced nuclear entry thus blocking its nuclear function. In our study, in contrast to the cytoplasmic localization of MTA1s, the C-terminal 33-amino acid peptide of MTA1s was localized in both the cytoplasm and nucleus (Fig. 3), where nuclear entry might be attributed to its small size and passive accumulation in the nucleus. The efficient repression of ERE-luc by this peptide led us to speculate whether this could be brought about by the peptide functioning as a mimetic of NR-boxes of the coactivator, preventing the binding of coactivators to the AF2 domain. We found proof-of-principle evidence of the repression of ERα transcription by the MTA1s peptide; the underlying mechanism involves competition and prevention of the recruitment of coactivators to the ligand-bound ERα. Consistent with this notion, the down-regulation of ERα transactivation activity was accompanied by an inhibitory effect of the MTA1s peptide on estrogen-induced proliferation of breast cancer cells in tissue culture- and animal-based systems.

Estrogens are a major inducer of cell proliferation in both normal and neoplastic breast epithelium (28) and mediate its effects via binding to high affinity receptors. ERα functions as an estrogen-activated transcription factor and is involved in the stimulation of estrogen target genes that modulate cell cycle progression and growth of breast epithelium. Excessive stimulation of the ER pathway due to increased hormonal secretion or increased levels of the receptor may lead to augmentation of cell proliferation and increases the risk of uncontrolled growth stimulation and cancer. Patients with breast cancer have higher levels of ERα expression than healthy subjects (29). Results from immunohistochemical studies of normal and cancerous tissue showed that ~20–30% of cells in the normal mammary gland are ER-positive (30, 31), but the ratio of ER-positive cells

significantly increases in proliferative diseases, implying an increased risk of tumorigenesis under conditions of increased ER expression. Approximately 50% of breast cancers are positive for the expression of ERα and respond to the mutagenic and proliferative effects of estrogen (32). The most widely used therapy for these breast tumors has been a class of drugs generally referred to as selective estrogen receptor modulators, which act as binding competitors to the ERs and block the effects of estrogens. One such drug is tamoxifen, which antagonizes the action of estrogens and is being used in both the prevention (33) and treatment of breast cancer (34). It is an efficient selective estrogen receptor modulator in the breast tissue, but it has a different mode of action in other tissues. For example, in endometrium and bone tissues, tamoxifen acts as an agonist, increasing the risk of endometrial cancer in patients (35). In addition to this, prolonged administration of tamoxifen has resulted in the development of resistance to its effects. Its slightly agonistic effects have even resulted in tumor regrowth (36).

In view of these complications, the identification of alternative therapeutic approaches to breast cancer therapy is of continued interest. One approach is to counteract the functions of ERα coactivators, which, on recruitment to ligand-bound ERα, are involved in bringing about chromatin modification to facilitate target gene regulation. These coactivator proteins have been implicated in disorders of the endocrine system and steroid-induced cancers. For instance, the coactivator AIB1 is found to be up-regulated in a high proportion of ERα-positive tumors (37). Similarly, enhanced PELP1 expression was observed in breast tumors (6). In view of these findings, abrogating the recruitment of coactivators by ligand-bound ERα may impair the stimulation of its target genes. In this context, we found that the NR-box-containing C-terminal peptide of MTA1s has antiestrogenic effects in breast cancer cells and may be useful in breast cancer therapy.

Acknowledgments—We thank Dr. Christopher J. Barnes for the streptavidin staining. We also thank Dr. Robert A. Newman and the Pharmaceutical Development Center Core Facility of M.D. Anderson Cancer Center for preparing liposomal formulation of our test peptides.

REFERENCES

1. Mangelsdorf, D. J., Thummel, C., Beato, M., Herrlich, P., Schutz, G., Umesono, K., Blumberg, B., Kastner, P., Mark, M., Chambon, P., and Evans, R. M. (1995) ***Cell*, 83,** 835–839
2. Tenenbaum, D. M., Wang, Y., Williams, S. P., and Sigler, P. B. (1998) *Proc. Natl. Acad. Sci. U. S. A.* **95,** 5998–6003
3. Shaffer, P. L., Jivan, A., Dollins, D. E., Claesseus, F., and Gewirth, D. T. (2004) *Proc. Natl. Acad. Sci. U. S. A.* **101,** 4758–4763
4. Singh, R. R., and Kumar R. (2005) *J. Cell. Biochem.* **96,** 490–505
5. Lonard, D. M., and O'Malley, B. W. (2005) *Trends Biochem. Sci.* **30,** 126–132
6. Vadlamudi, R. K., Wang, R.-A., Mazumdar, A., Kim, Y., Shin, J., Sahin, A., and Kumar, R. (2001) *J. Biol. Chem.* **276,** 38272–38279
7. McInerney, E. M., Rose, D. W., Flynn, S. E., Westin, S., Mullen, T. M., Krones, A., Inostroza, J., Torchia, J., Nolte, R. T., Assa-Munt, N., Milburn, M. V., Glass, C. K., and Rosenfeld, M. G. (1998) *Genes Dev.* **12,** 3357–3368
8. Chang, Y. C., Norris, J. D., Gron, H., Paige, L. A., Hamilton, P. T., Kenan, D. J., Fowlkes, D., and McDonnell, D. P. (1999) *Mol. Cell. Biol.* **19,** 8226–8239
9. Kumar, R., Wang, R. A., Mazumdar, A., Talukder, A. H., Mandal, M., Yang, Z., Bagheri-Yarmand, R., Sahin, A., Hortobagyi, G., Adam, L., Barnes, C. J., and Vadlamudi, R. K. (2002) *Nature* **418,** 654–657
10. Ogg, R. J., Kingsley, P. B., and Taylor, J. S. (1994) *J. Magn. Res. Ser. B* **104,** 1–10
11. Smallcombe, S. H., Patt, S. L., and Keifer, P. A. (1995) *J. Magn. Res. Ser. A* **117,** 295–303
12. Piotto, M., Saudek, V., and Sklenar, V. (1992) *J. Biomol. NMR* **2,** 661–665
13. Rance, M., Sorensen, O. W., Bodenhausen, G., Wagner, G., Ernst, R. R., and Wuthrich, K. (1983) *Biochem. Biophys. Res. Commun.* **117,** 479–485
14. Braunschweiler, L., and Ernst, R. R. (1983) *J. Magn. Res.* **53,** 521–528
15. Kumar, A., Ernst, R. R., and Wuthrich, K. (1980) *Biochem. Biophys. Res. Commun.* **95,** 1–6
16. Brunger, A. T. (1992) *X-PLOR Version 3.1. A System for X-ray Crystallography and NMR*, Yale University, New Haven, CT
17. Balasenthil, S. and Vadlamudi, R. K. (2003) *J. Biol. Chem.* **278,** 22119–22127
18. Vadlamudi, R. K., Adam, L., Wang, R. A., Mandal, M., Nguyen, D., Sahin, A., Chernoff, J., Hung, M. C., and Kumar, R. (2000) *J. Biol. Chem.* **275,** 36238–36244
19. Vadlamudi, R. K., Bagheri-Yarmand, R., Yang, Z., Balasenthil, S., Nguyen, D., Sahin, A. A., den Hollander, P., and Kumar, R. (2004) *Cancer Cell* **5,** 575–585
20. Wuthrich, K. (1986) *NMR of Proteins and Nucleic Acids*, John Wiley and Sons, New York, pp. 130–161
21. Warnmark, A., Treuter, E., Gustafsson, J. A., Hubbard, R. E., Brzozowski, A. M., and Pike, A. C. (2002) *J. Biol. Chem.* **277,** 21862–21868
22. Manavathi, B., Nair, S. S., Wang, R.-A., Kumar, R., and Vadlamudi, R. K. (2005) *Cancer Res.* **65,** 5571–5577
23. Tora, L., White, J., Brou, C., Tasset, D., Webster, N., Scheer, E., and Chambon, P. (1989) *Cell. Nov* **59,** 477–487
24. Tzukerman, M. T., Esty, A., Santiso-Mere, D., Danielian, P., Parker, M. G., Stein, R. B., Pike, J. W., and McDonnell, D. P. (1994) *Mol. Endocrinol.* **8,** 21–30
25. Shiau, A. K., Barstad, D., Loria, P. M., Cheng, L., Kushner, P. J., Agard, D. A., and Greene, G. L. (1998) *Cell* **95,** 927–937
26. Horwitz, K. B., Jackson, T. A., Bain, D. L., Richer, J. K., Takimoto, G. S., and Tung, L. (1996) *Mol. Endocrinol.* **10,** 1167–1177
27. Mazumdar, A., Wang, R. A., Mishra, S. K., Adam, L., Bagheri-Yarmand, R., Mandal, M., Vadlamudi, R. K., and Kumar, R. (2001) *Nat. Cell Biol.* **3,** 30–37
28. Pike, M. C., Krailo, M. O., Henderson, B. E., Casagrande, J. T., and Hoel, D. G. (1983) *Nature* **303,** 767–770
29. McGuire, W. L., Carbone, P. P., and Vollmer, E. P. (1975) *Estrogen Receptor in Human Breast Cancer*, pp. 57–72, Raven Press, New York
30. Khan, S. A., Rogers, M. A., Khurana, K. K., Meguid, M. M., and Numann, P. J. (1998) *J. Natl. Cancer. Inst.* **90,** 37–42
31. Shoker, B. S., Jarvis, C., and Clark, R. B. (1999) *Am. J. Pathol.* **155,** 184–185
32. Scot, J. A., and McGuire, W. L. (1991) in *Endocrine-Dependent Tumors* (Voight, K. D., and Knabe, C., eds) pp. 179–196, Raven Press, New York
33. Fisher, B., Costantino, J. P., Wickerham, D. L., Redmond, C. K., Kavanah, M., Cronin, W. M., Vogel, V., Robidoux, A., Dimitrov, N., Atkins, J., Daly, M., Wieand, S., Tan-Chiu, E., Ford, L., and Wolmark, N. (1998) *J. Natl. Cancer Inst.* **90,** 1371–1388
34. Cole, M. P., Jones, C. T., and Todd, I. D. (1971) *Br. J. Cancer.* **25,** 270–275
35. Fisher, B., Costantino, J. P., Redmond, C. K., Fisher, E. R., Wickerham, D. L., and Cronin, W. M. (1994) *J. Natl. Cancer Inst.* **86,** 527–537
36. Johnston, S. R. (1997) *Anticancer Drugs* **8,** 911–930
37. Anzick, S. L., Kononen, J., Walker, R. L., Azorsa, D. O., Tanner, M. M., Guan, X. Y., Sauter, G., Kallioniemi, O. P., Trent, J. M., and Meltzer, P. S. (1997) *Science* **27,** 965–968